Journal of the American Chemical Society

Two synthetic replicators compete to process a dynamic reagent pool

Tamara Kosikova and Douglas Philp*

School of Chemistry and EaStCHEM, University of St Andrews, North Haugh, St Andrews, KY16 9ST Fife, United Kingdom

*Corresponding author: d.philp@st-andrews.ac.uk

Abstract

Complementary building blocks, comprising a set of four aromatic aldehydes and a set of four nucleophiles—three anilines and one hydroxylamine—combine through condensation reactions to afford a dynamic covalent library (DCL) consisting of the 8 starting materials and 16 condensation products. One of the aldehydes, and, consequently, all of the DCL members derived from this compound, bears an amidopyridine recognition site. Exposure of this DCL to two maleimides, $\mathbf{M^p}$ and $\mathbf{M^m}$, each equipped with a carboxylic acid recognition site, results in the formation of a series of products through irreversible 1,3-dipolar cycloaddition reactions with the four nitrones present in the DCL. However, only the two cycloadducts in the product pool that incorporate both recognition sites, $\mathbf{T^p}$ and $\mathbf{T^m}$, are self-replicators that can harness the DCL as feedstock for their own formation, facilitating their own synthesis *via* autocatalytic and crosscatalytic pathways. The ability of these replicators to direct their own formation from the components present in the dynamic reagent pool in response to the input of instructions in the form of pre-formed replicators is demonstrated through a series of quantitative $^{19}F\{^1H\}$ NMR spectroscopy experiments. Simulations establish the critical relationships between the kinetic and thermodynamic parameters of the replicators, the initial reagent concentrations, and the presence or absence of the DCL and their influence on the competition between $\mathbf{T^p}$ and $\mathbf{T^m}$. Thereby, we establish the rules that govern the behavior of the competing replicators under conditions where their formation is coupled tightly to the processing of a DCL.

Introduction

Elucidating the pathways by which complex systems[1] emerged early in the history of the Earth provides a significant challenge[1a–e,2] for the discipline of chemistry. There are several schools of thought[3,4] regarding the mechanics of this process, including the appearance[4] of reaction networks assembled from small organic molecules that participate in interconnected catalytic cycles. Such networks have been suggested[4] as progenitors to life on Earth. Central to this metabolism-first theory of the origin of life is the ability to process[4] pools of reagents in a programmed and directed manner. This processing most likely involved significant energy input on the early Earth. In addition, another key requirement is the input of information that is necessary to direct the various chemical reactions within the network in an appropriate manner. A process of central importance to the transition[1a–e,2–5] from autonomous chemical networks to living systems is replication—that is, a process in which one molecular entity templates its own formation or those of others. Over the past 30 years, artificial replicating systems[6] have progressed from early examples of isolated self- and reciprocal[7,8] replicators to instructable networks[9] consisting of a number of replicators. Exploiting our burgeoning understanding of the principles that govern reactivity and information transfer within systems based on synthetic replicators, networks that express a range of functionalities beyond simple structural information transfer have been described—for example, Boolean logic operations,[10] error correction,[11] stereospecific[12] replication, creation of mechanically-interlocked[13] molecules, and initiation and propagation of reaction-diffusion fronts.[14]

We wish to develop reaction networks that are directed by replicators and which are capable of processing compositionally-complex mixtures of feedstocks. In order to achieve this goal, we must establish the basic design principles with respect to the interplay between replicator efficiency, network topology and feedstock availability. Dynamic covalent chemistry[15] (DCC) provides an excellent platform for the exploration of chemical networks that possess significant levels of connectivity between network components. DCC exploits simple building blocks bearing compatible reactive sites. Their pairwise combinations permit the creation of dynamic covalent libraries (DCLs) whose composition is under thermodynamic control. A DCL can be instructed[15,16] by the addition of an external agent, which drives the re-equilibration of the library towards a new composition based on the applied selection pressure. In the context of replicating systems, DCLs offer a unique platform on which to study template-directed processes under reaction conditions where replicators must process the dynamic pool of components in order to generate the building blocks required for their own syntheses.

Therefore, we regard systems in which a replicator network is coupled to a DCL as models with which to study the parameters required for the operation of systems that can process chemical

feedstocks in a programmed, yet autonomous, manner and serve as models for the transition from pools of simple chemical compounds to systems envisaged by metabolism-first theories of the origin of life. To date, however, relatively few studies have examined[7c,16a,b,d,17] the operation of replication processes embedded within or coupled to DCLs, and most examples have been limited to either a single replication process or replication processes that operate reversibly.

Previously, our laboratory[17c] and others[17a,b,d] have shown that there is a limit to the degree of amplification of particular constitutions that can be achieved in DCLs that are coupled to reversible replication phenomena operating under thermodynamic control. This limitation can be overcome by coupling[18] DCLs to kinetically-controlled irreversible replication processes that transfer material irreversibly out of the DCL. In this work, we examine the capacity of two competing replicators to process a dynamic reagent pool to direct their own formation and the dependence of the processing efficiency on the kinetic and thermodynamic parameters associated with the replicators and the experimental conditions, such as initial reagent concentration and the presence or absence of the DCL. A schematic representation of the processing of a DCL (dynamic reagent pool) by two competing replicators is shown in Figure 1. The dynamic exchange pool is constructed by combining two sets of four building blocks (**A** to **D** and **W** to **Z**) with complementary reactivities. The resulting reagent pool contains subsets of components that are capable of interacting (pale purple, derived from **A**) or reacting (dark green, derived from **Z**) with two target species—$\mathbf{M^p}$ (deep yellow) and $\mathbf{M^m}$ (pale yellow). The creation, from Set 1 and Set 2, of the dynamic exchange pool containing four compounds with the green reactive site (Figure 1) affords the system the opportunity to create a further eight compounds—four from the reaction with $\mathbf{M^p}$ and four from the reaction with $\mathbf{M^m}$. Of these eight compounds, only the two replicators labelled $\mathbf{T^p}$ and $\mathbf{T^m}$ in Figure 1, are capable of further processing the reagent pool to direct their own formation through autocatalytic template-directed pathways (autocatalytic cycles 1 and 2, Figure 1). The autocatalytic processing of **AZ** through these pathways into either replicator $\mathbf{T^p}$ or $\mathbf{T^m}$ results in its irreversible removal from the DCL, thereby creating the necessary driving force for the reconfiguration of this reagent pool.

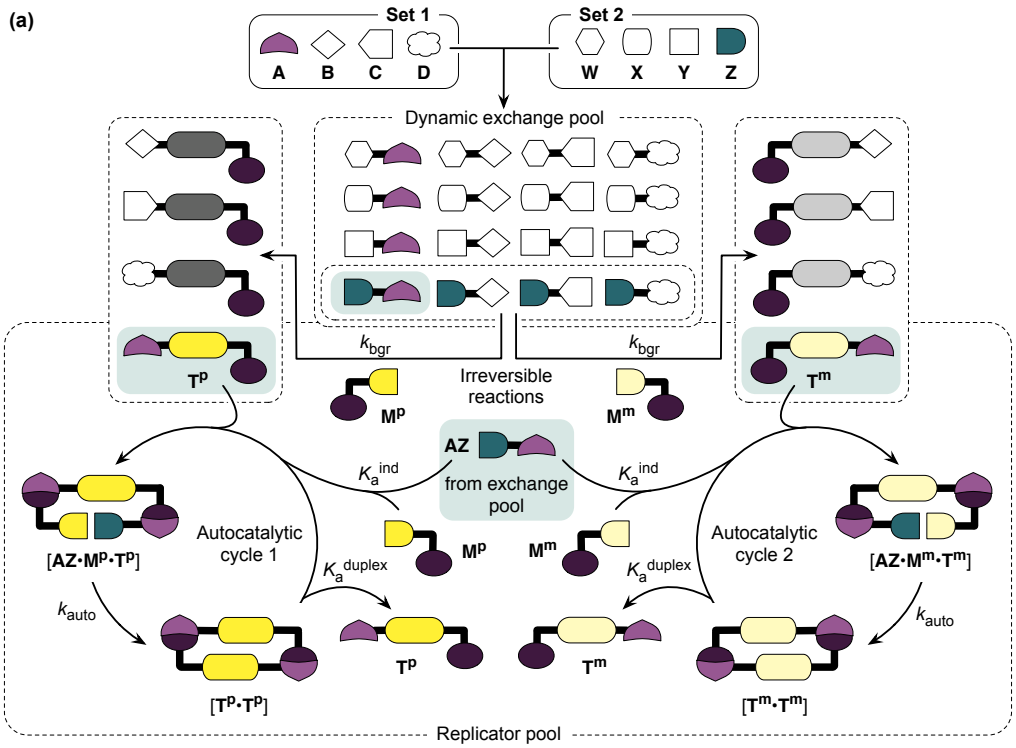

Figure 1. The combination of two sets of four building blocks gives rise to a dynamic exchange pool of 16 exchange pool members. Consequently, together with the 8 original reagents, the dynamic covalent library comprises 24 components in total. Certain members of the exchange pool possess a reactive site (dark green) that allows them to react irreversibly with the added targets, $\mathbf{M^p}$ and $\mathbf{M^m}$, while others possess a recognition site (light purple) that allows them to interact with $\mathbf{M^p}$ and $\mathbf{M^m}$ reversibly through non-covalent bonds. However, out of the eight products formed, only two ($\mathbf{T^p}$ and $\mathbf{T^m}$), formed by the reaction the targets with **AZ**, *i.e.*, the exchange pool member equipped with both the recognition site (pale purple) and the reactive site (dark green), are capable of initiating template-mediated self-replication cycles (cycles 1 and 2, respectively) driven by the formation of catalytically active ternary complexes [$\mathbf{AZ{\bullet}M^p{\bullet}T^p}$] and [$\mathbf{AZ{\bullet}M^m{\bullet}T^m}$]. The autocatalytic processes remove component **AZ** irreversibly from the exchange pool, processing the DCL to drive their own formation. For a discussion of the rate and association constants in the figure, see the main text. Note that the individual values of these kinetic and thermodynamic parameters for $\mathbf{T^p}$ and $\mathbf{T^m}$ are specific to each replicator and may differ from each other.

Design and implementation of a DCL coupled to two competing replicators

Previously, we have demonstrated[18,19] that an irreversible 1,3-dipolar cycloaddition reaction can be exploited to process a DCL containing nitrones and imines, either through a recognition-mediated reaction pathway[19] or through self-replication.[18] In this work, we exploit four aldehydes (**A** to **D**) and four nucleophiles (**W** to **Z**) (Figure 2a) in order to implement experimentally the model shown in Figure 1. The reactions of the aldehydes with the nucleophiles afford a dynamic reagent pool of 12 imines and 4 nitrones, together with the 8 starting materials themselves. The members of this DCL were selected to afford an exchange pool that contains a subset of components that possess a 6-methyl amidopyridine recognition site (Figure 2a, pale purple) and a subset of components that possess a nitrone reactive site (Figure 2a, dark green), which enable them to either interact or react with the added targets, that is, maleimides $\mathbf{M^p}$ and $\mathbf{M^m}$ (Figure 2b), which are each equipped with a carboxylic acid recognition site (Figure 2b, dark purple). However, only one compound in these two subsets lies within their intersection, namely, nitrone **AZ** (Figure 2a, pale green rectangle). This compound is capable of *both* interacting with $\mathbf{M^p}$ and $\mathbf{M^m}$ and reacting with them through irreversible 1,3-dipolar cycloaddition reactions. These reactions between nitrone **AZ** and the two maleimides create two templates, referred[20] to as $\mathbf{T^p}$ (Figures 2c and 3, deep yellow) and $\mathbf{T^m}$ (Figures 2c and 3, pale yellow), which were demonstrated previously to possess[21] the capacity to participate in two autocatalytic pathways (Figure 3), in which $\mathbf{T^p}$ and $\mathbf{T^m}$ catalyze their own formation. In addition, a crosscatalytic relationship exists between these templates, whereby $\mathbf{T^p}$ catalyzes the formation of $\mathbf{T^m}$ efficiently, but not *vice versa*. In previous work,[21] we demonstrated, using comprehensive kinetic analyses and density functional calculations, that the inability of $\mathbf{T^m}$ to template the formation of $\mathbf{T^p}$ is a direct result of the ability of $\mathbf{T^m}$ to sequester $\mathbf{T^p}$ in the [$\mathbf{T^p}$•$\mathbf{T^m}$] hetereoduplex and the comparatively low efficiency of the [**AZ**•$\mathbf{M^p}$•$\mathbf{T^m}$] ternary complex. Therefore, within the DCL, the syntheses of replicators $\mathbf{T^p}$ and $\mathbf{T^m}$ are driven by the reactions between **AZ** and the two maleimides $\mathbf{M^p}$ and $\mathbf{M^m}$. Consequently, we expect these processes to drive redistribution of the building blocks amongst the interconverting dynamic reagent pool. The presence of an aryl fluorine tag[22] on the four nucleophiles **W** to **Z** ensures that all library components derived from them (Figure 2c) can be identified and monitored readily using $^{19}F\{^1H\}$ NMR spectroscopy.

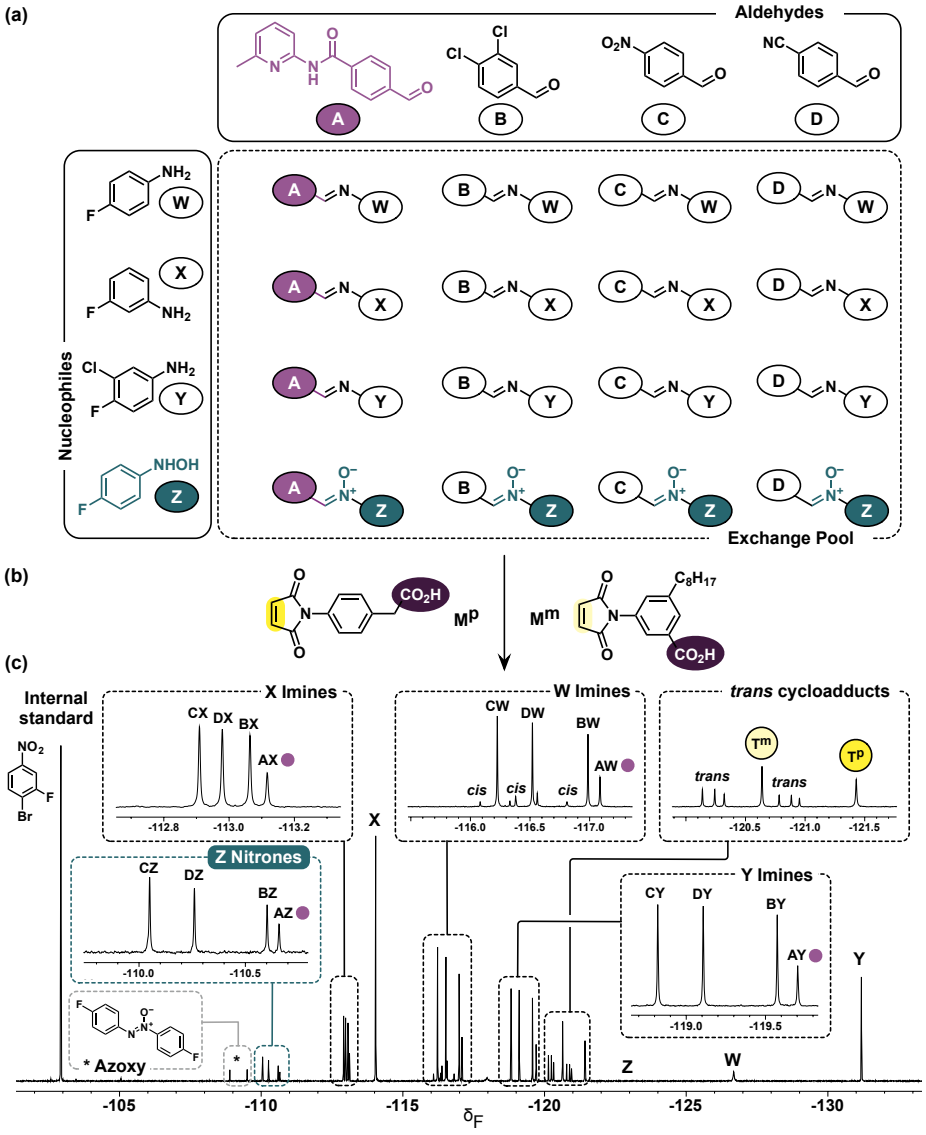

Figure 2. (a) A dynamic covalent library (DCL) is assembled from aldehydes **A** to **D**, which can react with anilines **W** to **Y** and hydroxylamine **Z** to produce an exchange pool that contains 12 imines and 4 nitrones. In this pool, only the four nitrones possess the reactive site (dark green) necessary for 1,3-dipolar cycloaddition reactions with maleimides. Similarly, only four exchange pool components formed by reaction with aldehyde **A** bear the 6-methyl amidopyridine recognition site (pale purple) that allow these compounds to interact non-covalently with $\mathbf{M^p}$ and $\mathbf{M^m}$. (b) Instruction of the DCL with maleimides $\mathbf{M^p}$ and $\mathbf{M^m}$, each bearing a carboxylic acid recognition site, transforms the exchange pool. Only the reactions of $\mathbf{M^p}$ with **AZ** and $\mathbf{M^m}$ with **AZ** result in the formation of products capable of directing their own formation *via* self-replication. (c) Example partial $^{19}F\{^1H\}$ NMR spectrum (282.4 MHz, CD_2Cl_2 saturated with *p*TSA monohydrate) of a DCL instructed with two maleimides $\mathbf{M^p}$ and $\mathbf{M^m}$ ([**A**] to [**D**] = [**W**] = [**Z**] = [$\mathbf{M^p}$] = [$\mathbf{M^m}$] = 10 mM) and containing 1-bromo-2-fluoro-4-nitrobenzene as internal standard, after seven days at 5 °C. The processing of the DCL produces various *trans* and *cis* cycloadducts; only $\mathbf{T^p}$ and $\mathbf{T^m}$ are capable of replication. Resonances marked with ● indicate compounds that contain an amidopyridine recognition site. The symbol * denotes the resonances arising from the azoxy side product.

When the components **A** to **D** and **W** to **Z** are first mixed, there are no condensation products present in the exchange pool, and, thus, this pool is a reservoir that can supply the building

blocks necessary for the formation of nitrone **AZ**. This DCL member is of particular interest since it possesses both recognition (6-methyl amidopyridine) and reactive (nitrone) sites and would be expected to react with both $\mathbf{M}^{p}$ and $\mathbf{M}^{m}$ through recognition-mediated pathways that are likely to be highly diastereoselective.[23] In addition to nitrone **AZ**, however, the DCL exchange pool also contains three additional nitrones, **BZ**, **CZ**, and **DZ**, which are capable of reacting with $\mathbf{M}^{p}$ and $\mathbf{M}^{m}$ through non-catalyzed, and, thus, significantly slower and less diastereoselective[23,24] bimolecular pathways. As a result, we envisaged that the self-replicating templates $\mathbf{T}^{p}$ and $\mathbf{T}^{m}$ would be able to process the reagent pool by selectively removing **AZ** from the DCL by its reactions with $\mathbf{M}^{p}$ or $\mathbf{M}^{m}$, in preference to all of the other possible cycloaddition products. In order to assess the ability of the competing replicators to process the dynamic reagent pool, we can examine the influence of the two irreversible, kinetically-controlled replication pathways on the composition of the DCL.

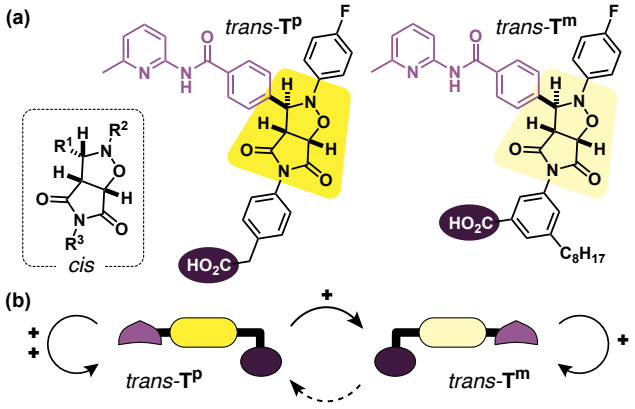

Figure 3. (a) Chemical structures of replicators *trans*-$\mathbf{T}^{p}$ and trans-$\mathbf{T}^{m}$, formed by the reactions of nitrone **AZ** with $\mathbf{M}^{p}$ and $\mathbf{M}^{m}$, respectively. The configuration of the three protons located on the isoxazolidine ring of the cycloadduct in the recognition-disabled *cis* diastereoisomer is illustrated in the dashed rectangle. (b) Cartoons illustrating the catalytic relationships between these two replicators. Efficiency: dashed line = low ($EM_{kinetic}$ < 5 M); + = medium (5 M < $EM_{kinetic}$ < 50 M); ++ high ($EM_{kinetic}$ > 50 M).

Results and Discussion

The first step in our analysis of the performance of replicators $\mathbf{T}^{p}$ and $\mathbf{T}^{m}$ within the DCL was to examine the composition of the dynamic exchange pool in the absence of any irreversible reaction processes (*i.e.*, in the absence of the maleimides and preformed replicators $\mathbf{T}^{p}$ and $\mathbf{T}^{m}$). This analysis is critical to establish the unperturbed equilibrium position of the DCL. Accordingly, we prepared an equimolar solution of all of the aldehydes and nucleophiles ([**A**] to [**D**] = [**W**] to [**Z**] = 10 mM) in CD_2Cl_2 that had previously been saturated with *p*-toluene sulfonic acid (*p*TSA). This sample was allowed to equilibrate at 5 °C (for details of DCL sample preparation and analysis by NMR, see Sections S1, S2, and S4) and its composition was

evaluated quantitatively by 282.4 MHz $^{19}F\{^{1}H\}$ NMR spectroscopy. The results reveal that while the condensation reactions begin to generate[25] the exchange pool components immediately after mixing, the library takes several days to fully reach its equilibrium position (Figure 4).

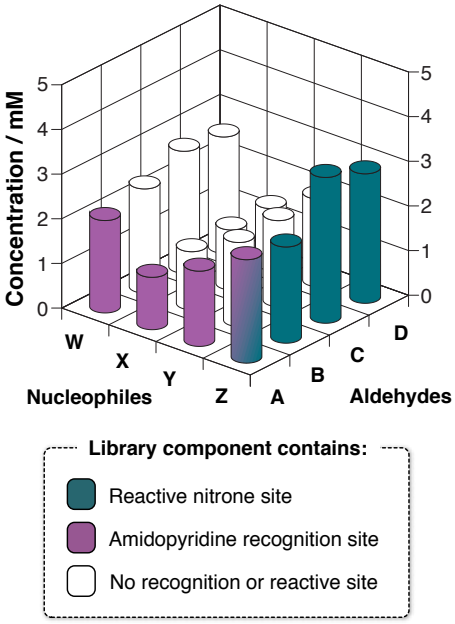

Figure 4. Distribution of a dynamic covalent library, assembled from aldehydes **A** to **D** and nucleophiles **W** to **Z**, in the absence of any reactive maleimide components ([**A**] to [**D**] = [**W**] to [**Z**] = 10 mM, in CD_2Cl_2 saturated with *p*TSA) as determined by 282.4 MHz $^{19}F\{^{1}H\}$ NMR spectroscopy after seven days. Only four library components, nitrones **AZ** to **DZ**, possess the nitrone reactive site (dark green) necessary for 1,3-dipolar cycloaddition reactions with maleimides. Similarly, only four exchange pool components formed by reactions with aldehyde **A** bear the 6-methyl amidopyridine recognition site (pale purple). Exchange pool components lacking both the reactive and recognition site are colored white.

The equilibrium position for the formation of nitrones from hydroxylamine **Z** after seven days lies far to the side of the products—there is almost complete conversion (>99%) to the corresponding condensation products. Distribution of **Z** across the four nitrones reflects the electron-withdrawing ability of the functional groups present on each aldehyde. Nitrone **CZ** is formed at the highest concentration ([**CZ**] = 3.3 mM), closely followed by nitrone **DZ** ([**DZ**] = 2.9 mM). Nitrones **AZ** and **BZ** are formed from less electrophilic aldehydes and are present at concentration of only 2.3 mM and 2.2 mM, respectively. The second-best nucleophile in the system is *p*-fluoroaniline **W**, and this compound shows an overall conversion of 88% to the corresponding imine condensation products. In comparison to **W** and **Z**, at equilibrium, 4-fluoro-3-chloroaniline **Y** reached only 72% conversion, while the least reactive nucleophile, 3-fluoroaniline **X**, was only 49% converted into **X**-containing imine products. Comparison of the

composition after two and seven days showed <5% difference[26] in concentration for each library component.

Processing of the DCL by competing replicators $\mathbf{T^p}$ and $\mathbf{T^m}$

Having established the equilibrium position for the DCL successfully, we were now in a position to examine the behavior of the replicators $\mathbf{T^p}$ and $\mathbf{T^m}$ within the dynamic environment of the DCL and compare this behavior to that described previously[21] under conditions that were entirely kinetically-controlled—that is, conditions where the maleimides $\mathbf{M^p}$ and $\mathbf{M^m}$ can react with nitrone **AZ** only, *i.e.*, the DCL is absent. To this end, a sample of the DCL was prepared from components **A** to **D** and **W** to **Z** in CD_2Cl_2 saturated with *p*TSA. In addition, this mixture also contained the two maleimides $\mathbf{M^p}$ and $\mathbf{M^m}$. The composition of this mixture ([**A**] to [**D**] = [**W**] to [**Z**] = [$\mathbf{M^p}$] = [$\mathbf{M^m}$] =10 mM) was allowed to evolve in a thermally controlled water bath at 5 °C for seven days. After two (Figure 5a(i)) and seven days (Figure 5b(i)), the composition of the library was determined quantitatively by 282.4 MHz $^{19}F\{^1H\}$ NMR spectroscopy.

After two days, *trans*-$\mathbf{T^p}$ and *trans*-$\mathbf{T^m}$ reached concentrations of 0.86 mM and 1.13 mM, respectively, representing 20% conversion of **AZ** into cycloadducts—the ratio of [$\mathbf{T^m}$]/[$\mathbf{T^p}$] was 1.3. This value is similar to the [$\mathbf{T^m}$]/[$\mathbf{T^p}$] ratio (1.2) observed[21] previously in a kinetically-controlled competition experiment after 16 h. The *trans* cycloadducts derived from $\mathbf{M^p}$ that bear only one recognition site and, therefore, cannot replicate (*trans*-$\mathbf{T^pB}$, *trans*-$\mathbf{T^pC}$, and *trans*-$\mathbf{T^pD}$) were present at a combined concentration of 0.70 mM, whereas the corresponding *trans* cycloadducts derived from $\mathbf{M^m}$ were formed more efficiently, reaching a combined concentration of 1.19 mM. At this stage, therefore, the concentration of the self-replicating template $\mathbf{T^m}$ present in solution is marginally lower than the combined concentrations of the other *trans* cycloadducts, namely *trans*-$\mathbf{T^mB}$, *trans*-$\mathbf{T^mC}$, and *trans*-$\mathbf{T^mD}$ cycloadducts. Since maleimide $\mathbf{M^m}$ is associated with a higher bimolecular rate constant (k_{bgr}) for cycloaddition reaction involving nitrone **AZ** than maleimide $\mathbf{M^p}$, this observation is not entirely surprising. Despite the similarities in the ratio of the two replicators ([$\mathbf{T^m}$]/[$\mathbf{T^p}$]) formed from the DCL to that under strictly kinetically-controlled, the conversion of **Z** to replicating templates within the DCL was significantly lower. In fact, ~6 mM of hydroxylamine **Z** remained distributed among the four nitrones after two days (no free **Z** was detected). By contrast, in the absence of the DCL, the conversion to cycloadducts was higher—exceeding 50% after 16 h.

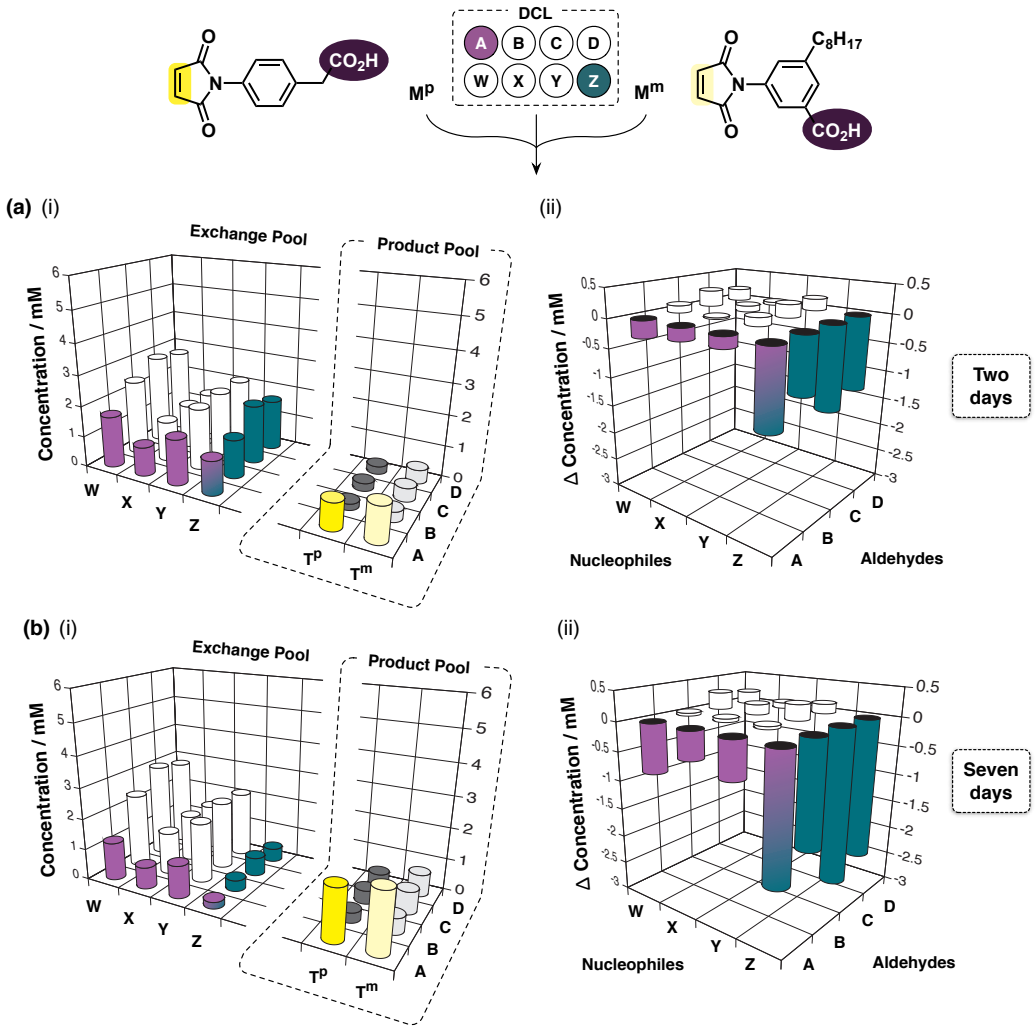

Figure 5. A DCL, assembled from components **A** to **D** and **W** to **Z**, was instructed with two recognition-enabled maleimides: $\mathbf{M^p}$ and $\mathbf{M^m}$. The graphs show the (i) composition of the exchange pool and the *trans* product pool, where *trans*-$\mathbf{T^p}$ is shown in yellow and *trans*-$\mathbf{T^m}$ in pale yellow, as determined by 282.4 MHz $^{19}F\{^1H\}$ NMR spectroscopy, relative to 1-bromo-2-fluoro-4-nitrobenzene as an internal standard ([**A**] to [**D**] = [**W**] to [**Z**] = [$\mathbf{M^p}$] = [$\mathbf{M^m}$] = 10 mM, in CD_2Cl_2 saturated with *p*TSA) after (a) two and (b) seven days at 5 °C. The recognition-disabled cycloadducts formed by the reaction of $\mathbf{M^p}$ and $\mathbf{M^m}$ with nitrones **BZ**, **CZ**, and **DZ** are shown in dark and light gray, respectively. (ii) Changes in the concentrations of the dynamic exchange pool components relative to the exchange pool composition determined in the control library (no maleimides) after (a) two days and (b) seven days. Components labeled pale purple possess the 6-methyl amidopyridine recognition site, while those in dark green are equipped with a reactive nitrone site. Exchange pool components lacking the reactive and recognition sites are colored white.

In order to determine the impact of the addition of the two recognition-enabled maleimides on the distribution of the DCL, the exchange pool composition after two days was compared to the exchange pool equilibrium composition observed in the absence of maleimides (Figure 5a(ii)). As expected, imines incorporating the 6-methyl amidopyridine recognition site (*i.e.*, imines derived from aldehyde **A**) decreased in concentration in the DCL reacted with $\mathbf{M^p}$ and $\mathbf{M^m}$ relative to the exchange pool on its own. This decrease represents the outcome of library re-equilibration taking place in order to compensate for the decreasing amount of

reactive nitrones present in the system—in particular nitrone **AZ**. Specifically, component **A** is gradually being released from its 'storage' in imines **AW**, **AX**, and **AY** and is transferred into nitrone **AZ**. This DCL component is consumed at the fastest rate as the replicators $\mathbf{T^p}$ and $\mathbf{T^m}$ process the library. These processes, which redistribute **A**, also result in the release of anilines **W**, **X**, and **Y** from imines **AW**, **AX**, and **AY**, respectively. Consequently, the concentrations of the imines formed by condensation of **W**, **X** and **Y** with aldehydes **B**, **C**, and **D** increase. As a result of the irreversible nature of the cycloadditions that remove nitrones from the DCL, all four reactive nitrones are depleted over time, albeit at significantly different rates.

Examination of the product pool after seven days (Figure 5b(i)) revealed further increases in the concentrations of *trans*-$\mathbf{T^p}$ and *trans*-$\mathbf{T^m}$ to 1.65 mM and 1.91 mM, respectively (36% conversion overall). The slight decrease in the resulting [$\mathbf{T^m}$]/[$\mathbf{T^p}$] ratio from 1.3 to 1.2 can be rationalized by a gradual decline in the efficiency of both recognition-mediated replication processes over time as the components required for their formation are progressively depleted. Thus, the initially enhanced imbalance between the replicators is eroded. Nevertheless, this value is again comparable to the [$\mathbf{T^m}$]/[$\mathbf{T^p}$] ratio of 1.2 observed[21] for the two replicators under kinetically-controlled conditions after 16 h. Between two and seven days, the total non-recognition *trans* cycloadducts formed from $\mathbf{M^p}$ have increased to a combined concentration of 1.2 mM. Similarly, the recognition-disabled *trans* cycloadducts derived from maleimide $\mathbf{M^m}$ continued to form at a faster rate than those from $\mathbf{M^p}$, reaching an overall concentration of 1.9 mM. After seven days, only 1.61 mM of **Z**-containing nitrones remained available in their unreacted form in the DCL. Figure 5b(ii) illustrates the changes observed in the concentrations of the exchange pool components after seven days as determined relative to the library pool without any added maleimides. The magnitudes of the perturbations in the library are noticeably larger after seven days than after two days.

Analysis of the DCL treated with maleimides $\mathbf{M^p}$ and $\mathbf{M^m}$ provides us with an understanding of the ability of replicators $\mathbf{T^p}$ and $\mathbf{T^m}$ to process the dynamic reagent pool in the absence of instructional preformed template. However, minimal replicators, such as $\mathbf{T^p}$ and $\mathbf{T^m}$, are catalysts for their own formation and, thus, the addition of a quantity of one or both of these replicators[27] at $t = 0$ will result in an enhancement in the production of the added replicator at early time points. Consequently, we envisaged that the degree of library processing observed in response to the actions of the two replicators could be altered by instructional inputs to the DCL in the form of preformed templates. Through these template-instructed experiments, we can determine the ability of each replicator ($\mathbf{T^p}$ or $\mathbf{T^m}$) to process the DCL to its advantage as a function of the added template and compare the outcomes to those observed under kinetically

controlled conditions. Accordingly, we prepared three DCL samples from components **A** to **D** and **W** to **Z** in CD_2Cl_2 saturated with *p*TSA. In addition to the two maleimides $\mathbf{M^p}$ and $\mathbf{M^m}$, these three samples also contained $\mathbf{T^p}$, $\mathbf{T^m}$, and both $\mathbf{T^p}$ and $\mathbf{T^m}$, respectively. The compositions of these mixtures ([**A**] to [**D**] = [**W**] to [**Z**] = [$\mathbf{M^p}$] = [$\mathbf{M^m}$] =10 mM, [instructional template] = 1 mM) were allowed to evolve in a thermally controlled water bath at 5 °C for seven days. Figure 6a provides a comparison of the ratios of [$\mathbf{T^m}$]/[$\mathbf{T^p}$] determined in the three template-instructed DCLs incorporating maleimides $\mathbf{M^m}$ and $\mathbf{M^p}$, after both two (filled squares) and seven (open squares) days, compared to the ratios determined for the uninstructed experiment after the same time period.

Both *trans*-$\mathbf{T^p}$ and *trans*-$\mathbf{T^m}$ were formed at higher concentrations in the three template-instructed experiments—reaching combined conversions of 35%, 26%, and 37% after two days—when compared to the DCL containing no added template (20% conversion to *trans*-$\mathbf{T^p}$ and *trans*-$\mathbf{T^m}$). In the presence of preformed 10 mol% of *trans*-$\mathbf{T^p}$, the [$\mathbf{T^m}$]/[$\mathbf{T^p}$] ratio decreased as a result of the higher catalytic efficiency[21] of $\mathbf{T^p}$ formation on $\mathbf{T^p}$ template ($EM_{kinetic}$ = 64.0 M) compared to the formation[21] of $\mathbf{T^m}$ on $\mathbf{T^p}$ ($EM_{kinetic}$ = 18.3 M). The ratio determined in the presence of $\mathbf{T^p}$ remained virtually unchanged after seven days. In the presence of *trans*-$\mathbf{T^m}$, a marked increase in the [$\mathbf{T^m}$]/[$\mathbf{T^p}$] ratio relative to that determined in the template-uninstructed experiment was observed, particularly after two days. This increase is in agreement with the catalytic efficiencies determined for the two template-directed pathways that can operate in this instructed scenario—that is, the formation of $\mathbf{T^m}$ on $\mathbf{T^m}$ is associated[21] with an $EM_{kinetic}$ of 9.47 M, whereas the formation of $\mathbf{T^p}$ on the cross-catalytic template $\mathbf{T^m}$ is significantly less efficient.[21] The initial advantage afforded to $\mathbf{T^m}$ after two days, arising as a result of its inability to cross-catalyze the formation of $\mathbf{T^p}$ efficiently, is eroded markedly over time. The presence of instructing template should exert the strongest effect on the processing of the reagent pool at earlier reaction time points, during which self-replicating reactions generally proceed with lower efficiency as a result of the absence of appropriate template. Simultaneous addition of both templates resulted in a ratio of [$\mathbf{T^m}$]/[$\mathbf{T^p}$] that is similar to that observed in the experiment instructed by $\mathbf{T^p}$ only. The slight excess of $\mathbf{T^m}$ observed in this experiment is directly related to the fact that $\mathbf{T^m}$ replicator is formed through two efficient catalytic pathways—one autocatalytic ($\mathbf{T^m} \rightarrow \mathbf{T^m}$) and one crosscatalytic ($\mathbf{T^p} \rightarrow \mathbf{T^m}$)—whereas $\mathbf{T^p}$, although a more efficient replicator in isolation, is formed only *via* one efficient autocatalytic pathway ($\mathbf{T^p} \rightarrow \mathbf{T^p}$).

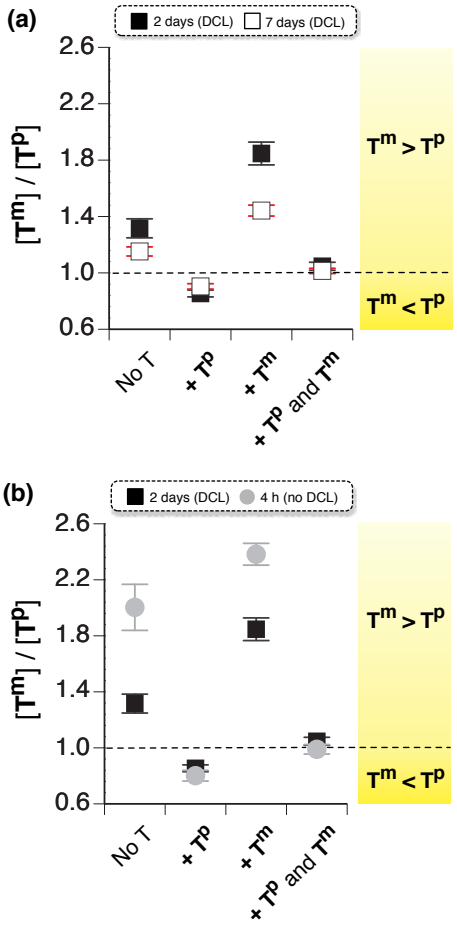

Figure 6. (a) The impact of instructing the DCL, assembled from components **A** to **D** and **W** to **Z** and both maleimides ($\mathbf{M^p}$ and $\mathbf{M^m}$), with preformed template (10 mol% added at $t = 0$ h) on the $[\mathbf{T^m}]/[\mathbf{T^p}]$ ratio after 2 days (black squares) and 7 days (white squares). All concentrations were determined by 282.4 MHz $^{19}F\{^1H\}$ NMR spectroscopy relative to 1-bromo-2-fluoro-4-nitrobenzene as an internal standard ([**A**] to [**D**] = [**W**] to [**Z**] = $[\mathbf{M^p}]$ = $[\mathbf{M^m}]$ = 10 mM, in CD_2Cl_2 saturated with *p*TSA, 5 °C. (b) Comparison of the $[\mathbf{T^m}]/[\mathbf{T^p}]$ ratios observed within the environment of a DCL after 2 days and in the absence of DCL ([**AZ**] = $[\mathbf{M^p}]$ = $[\mathbf{M^m}]$ = 5 mM, in $CDCl_3$, 5 °C; data taken from Ref. [21]) after 4 h as a function of the added preformed template. In both cases, the yellow shaded rectangle indicates the regions where the $[\mathbf{T^m}]/[\mathbf{T^p}]$ ratios are greater than 1 and *vice versa*. For details of error estimation, please see Section S2.2.

Next, we compared qualitatively the performance of the network under conditions where both kinetic and dynamic selection contributed to the processing of the reagent pool by the replicators (Figure 6a) to its performance[21] in a scenario (Figure 6b) where only kinetic selection contributed. The results reveal strong similarities in the observed trends in the $[\mathbf{T^m}]/[\mathbf{T^p}]$ ratios. In the absence of any preformed template (Figure 6b), replicator $\mathbf{T^m}$ is always present at a higher concentration than $\mathbf{T^p}$ at both reaction times examined—irrespective of whether selection was kinetic-only or both kinetic and dynamic. In addition, the selectivities determined in the presence of $\mathbf{T^p}$ and both $\mathbf{T^p}$ and $\mathbf{T^m}$ were almost identical in the presence and absence of the DCL. Finally, under both selection regimes, the highest selectivity was achieved

in the $\mathbf{T^m}$-instructed experiment—under kinetic and dynamic selection, the [$\mathbf{T^m}$]/[$\mathbf{T^p}$] ratio reached 1.85 after 2 days, and under kinetic selection only it was 2.38 after 4 h.[28] Overall, it is clear that replicator $\mathbf{T^m}$, despite possessing lower catalytic prowess in isolation, outperforms replicator $\mathbf{T^p}$ in the competition for the shared resource, nitrone **AZ**, in three experimental conditions out of four.

Coupling the network of two interconnected and competing self-replicators tightly with the dynamic reagent pool forces $\mathbf{T^p}$ and $\mathbf{T^m}$ to operate in an environment where they must drive the formation of **AZ** from components distributed across the entire library—*i.e.*, the nitrone required for their formation must itself be formed first through dynamic covalent exchange reactions. In this environment, we envisaged, that the replicator capable of initiating an autocatalytic cycle at lower template concentrations would process **AZ** faster, thus enhancing its own formation at the expense of the other template. However, the results show that the relative abilities of replicators $\mathbf{T^p}$ and $\mathbf{T^m}$ to process the dynamic reagent pool are very similar to those observed under kinetically controlled conditions. By contrast, the absolute abilities of the two replicators to process the dynamic building blocks were reduced within a DCL when compared to the abilities of the two replicators to process **AZ** in the absence of the DCL, as manifested by the lower conversions of **AZ** to $\mathbf{T^p}$ and $\mathbf{T^m}$. In order to elucidate the rules that govern the processing of the dynamic reagent pool by the two competing replicators, and to compare how these rules might differ from those operating under kinetic selection only, we turned to kinetic simulations.

Exploring the parameter space through kinetic simulations

The experimental system described here, incorporating replicators $\mathbf{T^p}$ and $\mathbf{T^m}$, is characterized[21] by a set of specific kinetic and thermodynamic parameters. Consequently, although it provides a proof-of-principle in terms of the processing of a DCL by two competing replicators, it does not lend itself easily to an exploration of the parameter space that such systems can access. For this reason, we were interested in exploiting kinetic simulations to probe how the behavior of a network containing two competing replicators, only one of which possesses efficient cross-catalytic activity, is affected by changes in certain key parameters—ranging from those that describe replication efficiency (kinetic effective molarity, $EM_{kinetic}$; thermodynamic effective molarity, EM_{thermo}) to reaction parameters, such as initial concentration.

As the first step in these simulations, we constructed a kinetic model that included the reactions[29] leading to the construction of the exchange pool from aldehydes, **A** to **D**, and

nucleophiles, **W** to **Z**, in order to model the dynamic exchange conditions. This model was constructed by identifying the trends in reactivity of the components **A** to **D** and **W** to **Z** and incorporating these trends into the model in such a way that the model can simulate the behavior of the exchange pool in the absence of any maleimides (Figures S2 and S3) observed experimentally (see Figure 4). In the next step, the reactions and interactions associated with the two replicators (for details, see the Supporting Information) were incorporated into the model. For ease of analysis, the simulations were performed using two replicators, **R1** and **R2**, whose catalytic relationships mirror those of the experimental network, but whose kinetic parameters are more amenable to systematic variation (Figure 7).

Our simulations focused on the interplay between three key parameters. The parameter $EM_{kinetic}$ captures the catalytic ability of and individual replicator. Thus, by varying the ratio of $EM_{kinetic}$ for **R2** and **R1** we capture the effect of making one replicator much more catalytically efficient than the other. We selected values for this ratio of 0.1, 1.0, and 10 in our simulations (conditions A to C, Figure 7a). The parameter EM_{thermo} captures autocatalyst availability as it is a measure of the stability of the replicator duplex. Strong duplexes reduce the amount of catalytically-active monomeric replicator in solution. Thus, by varying the ratio of EM_{thermo} for **R2** and **R1** we capture the effect of making one replicator much more available in solution than the other. We selected values for this ratio of 0.1, 1.0, and 10 in our simulations (conditions I–III, Figure 7a). Finally, the relationship between the K_d of individual binding events and the initial concentration of the reagents ($[C]_{Initial}$) determines whether the assembly of key complexes in the catalytic cycles is favored or disfavored. We chose to examine a range of concentration that spanned approximately two orders of magnitude from below the K_d for all of the individual binding events to well above the K_d for all of the individual binding events (Figure 7c). For the central condition IIB (Figure 7b), other parameter values were chosen such that replicators **R1** is formed more slowly by a bimolecular pathway (*i.e.*, **R1** has a lower k_{bgr}), has a lower autocatalytic rate constant (k_{auto}), a weaker product duplex (K_a^{duplex}) and weaker individual binding events (K_a^{ind}) than **R2**. In order to avoid an excessively large number of simulations, the parameters relating to the crosscatalytic pathways were kept constant (Figure 7b). As with the experimental system studied (where the synthesis of $\mathbf{T^m}$ is catalyzed efficiently by $\mathbf{T^p}$ but not *vice versa*), only one of the cross-catalytic pathways (the formation of **R2** templated by **R1**) was efficient. Full details of the simulations and example simulation scripts can be found in the Supporting Information (Sections S3 and S5). Taken together, the variation of $[C]_{Initial}$ (6 values), $EM_{kinetic}$ (3 values) and EM_{thermo} (3 values) afforded a data set containing 54 individual simulations in the presence of the DCL and a corresponding set of 54 individual

simulations where the DCL was absent, which we then analyzed to identify trends in the network behavior. We chose to examine the ratio of [**R2**]/[**R1**] as a marker of the efficiencies of the two replicators in processing **AZ** to drive their own syntheses. These results are summarized in Figure 8.

(a)

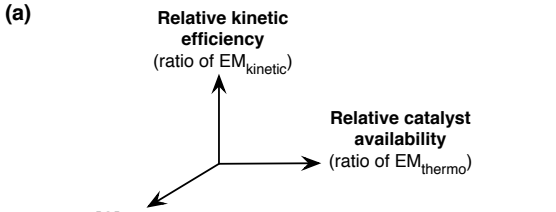

Ratio of $EM_{kinetic}$ R2/R1	Ratio of EM_{thermo} R2/R1: 0.1	1	10
0.1	IA	IIA	IIIA
1	IB	**IIB**	IIIB
10	IC	IIC	IIIC

(b)	R1	R2	Parameter ratio R2/R1
k_{bgr} / 10^{-4} M^{-1} s^{-1}	1.00	1.50	1.5
k_{auto} / 10^{-4} s^{-1}	100	150	1.5
$EM_{kinetic}$ / M	100	100	**1.0**
K_a^{duplex} / 10^6 M^{-1}	30.0	270	9.0
K_a^{ind} / M^{-1}	1000	3000	3.0
EM_{thermo}	30.0	30.0	**1.0**
k_{cross} / 10^{-4} s^{-1}	5.00	15.0	3.0
$EM_{kinetic}$ (cross) / M	5.00	10.0	2.0

(c)

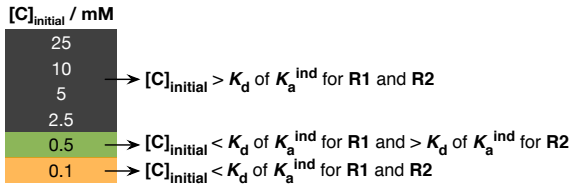

Figure 7. (a) Overview of kinetic simulations probing the influence of relative catalyst availability (EM_{thermo}, conditions I to III) and relative catalytic efficiency ($EM_{kinetic}$, conditions A to C) on the ratio of [**R2**]/[**R1**] formed in the presence of a DCL and in its absence. (b) Simulation IIB represents the central condition in which the thermodynamic and kinetic parameters are selected such that the ratios of both EM_{thermo} and $EM_{kinetic}$ for **R2**/**R1** are 1. (c) Simulated initial concentrations of reagents reflect a range of regimes in regard to the efficiency of the recognition-mediated processes. The rate and equilibrium constants shown in this figure match those introduced in Figure 1. Parameters k_{cross} and $EM_{kinetic}$ (cross) represent the rate constants and effective kinetic molarities associated with each of the crosscatalytic pathways.

Examination of the simulation set (Figure 8a) where $[C]_{initial}$ (= 2.5 mM) is above[30] the K_d for all of the individual binding events, reveals marked similarities between the behavior of the network in the presence (gray cylinders, Figure 8a) and in the absence (white cylinders, Figure 8a) of the DCL—measured in terms of the [**R2**]/[**R1**] ratio. In all 18 of the simulated conditions, the [**R2**]/[**R1**] ratio does not exceed 30. In condition IIB, where the ratios of both EM_{thermo} and $EM_{kinetic}$ for **R2**/**R1** are set to 1.0, the ratio of [**R2**]/[**R1**] is biased towards **R2**—[**R2**]/[**R1**] is 12.1 within the DCL and 7.3 in its absence—as a result of the higher k_{bgr} and k_{auto}

for replicator **R2** and its higher K_a^{ind}. The highest [**R2**]/[**R1**] ratios within the DCL and under kinetic selection only are 30 and 21, and are observed under condition IC in each case (highlighted in blue). By contrast, the lowest [**R2**]/[**R1**] ratios in the presence of the DCL and under kinetic selection only are 0.47 and 0.53, and are observed under condition IIIA in each case (highlighted in red). These two extremes identify the conditions under which **R2** and **R1**, respectively, display the highest relative abilities to process the reagents for their own syntheses.

The simulation set (Figure 8b) where $[C]_{initial}$ (= 0.5 mM) differs from the previous scenario in that the $[C]_{initial}$ is above the K_d for the individual binding events associated with **R2**, but below the K_d for those associated with **R1**. This lower initial concentration resulted in marked differences between this dataset and that shown in Figure 8a. In addition, this dataset also reveals more significant differences between the behavior of the network in the presence and in the absence of the DCL—once again measured in terms of [**R2**]/[**R1**] ratio. In this case, the [**R2**]/[**R1**] ratio in the 18 simulated conditions is as high as 50 in the presence of the DCL and as high as 31 under kinetic selection only (highlighted in blue, Figure 8). These ratios are observed under condition IC and IIC, respectively. By contrast, the lowest [**R2**]/[**R1**] ratios in the presence of the DCL and under kinetic selection only are both 0.53 and are, in common with the previous dataset, observed under condition IIIA (highlighted in red). When these simulations, at $[C]_{initial}$ = 0.5 mM, are compared to the simulations at $[C]_{initial}$ = 2.5 mM or above (for simulations $[C]_{initial}$ = 5 to 25 mM, see the Supporting Information), the values of [**R2**]/[**R1**] span a considerably larger range, indicating that **R2**, *i.e.*, the replicator with the higher K_a^{ind}, outperforms significantly **R1** in the competition for **AZ**. These results can be explained by the fact that at $[C]_{initial}$ of 0.5 mM, the recognition-mediated processes involving **R2** and **M2** proceed more efficiently than those involving **R1** and **M1**. By contrast, at $[C]_{initial}$ of 2.5 mM and above, the K_d of the individual binding events for both **R1** and **R2** are all above $[C]_{initial}$, and, therefore, all recognition processes can operate with comparable relative efficiency. Consequently, the advantage afforded to **R2** at low $[C]_{initial}$ diminishes progressively as $[C]_{initial}$ increases. Moreover, as $[C]_{initial}$ increases, the proportion of the products incapable of directing their formation *via* recognition-mediated pathways relative to **R1** and **R2** in the system increases owing to the increase in the background reaction rates.

Considering the simulation set (Figure 8c) where $[C]_{initial}$ (= 0.1 mM) is below the K_d for all of the individual binding events, the behavior of the network in the presence and in the absence of the DCL—measured in terms of [**R2**]/[**R1**]—shows marked differences to both of the other two scenarios described above. It is immediately apparent that, unlike in the two

preceding datasets, the range of simulated [**R2**]/[**R1**] values is considerably larger in the absence of the DCL than in its presence. The [**R2**]/[**R1**] ratios determined in the presence of the DCL at $[C]_{initial}$ = 0.5 mM are virtually all higher than those seen at $[C]_{initial}$ = 0.1 mM. By contrast, the ratios observed in the absence of the DCL at $[C]_{initial}$ = 0.5 mM are all lower than those seen at $[C]_{initial}$ = 0.1 mM. Consequently, the highest [**R2**]/[**R1**] ratio of 51 (highlighted in blue, Figure 8c) in these 18 simulated conditions is observed under kinetic selection only. The highest [**R2**]/[**R1**] ratio within the DCL is considerably lower, at 28 (highlighted in blue, Figure 8c). Nonetheless, in both selection regimes, the highest preference for **R2** is again found under condition IC. By contrast, the lowest [**R2**]/[**R1**] ratios within the DCL and in its absence are 1.3 and 0.58, respectively, and are observed in condition IIIA (highlighted in red).

It is notable that, with the exception of $[C]_{initial}$ = 0.1 mM, the simulated values of [**R2**]/[**R1**] in the presence of the DCL are higher than those simulated in the presence of kinetic control only. A selection regime driven by a combination of dynamic and kinetic control differs from one driven by kinetic selection only in that hydroxylamine **Z** is distributed amongst four nitrones (or present in its unreacted form), as opposed to being fully preformed. Consequently, the effective concentration of **AZ** available for reactions with the maleimides is comparatively lower (see Figure S4 for changes in **AZ** concentration as a function of $[C]_{initial}$) in the DCL regime. In the simulated DCL at $[C]_{initial}$ of 10 mM, for example, even if hydroxylamine **Z** has reacted fully to produce nitrones **AZ** to **DZ**, the concentration of the key nitrone **AZ** is *ca.* 4× smaller than the value of $[C]_{initial}$ as a consequence of its distribution within the four nitrones. The reduced availability of **AZ**, in turn, means that the system favors more strongly the formation of products that are derived from complexes that bind more tightly—in this case those involving **R2**. Overall, the outcome in the presence of the DCL is therefore shifted with respect to that obtained in the absence of the DCL when it reaches the threshold at which the recognition-mediated processes involving both **R1** and **R2** operate inefficiently.

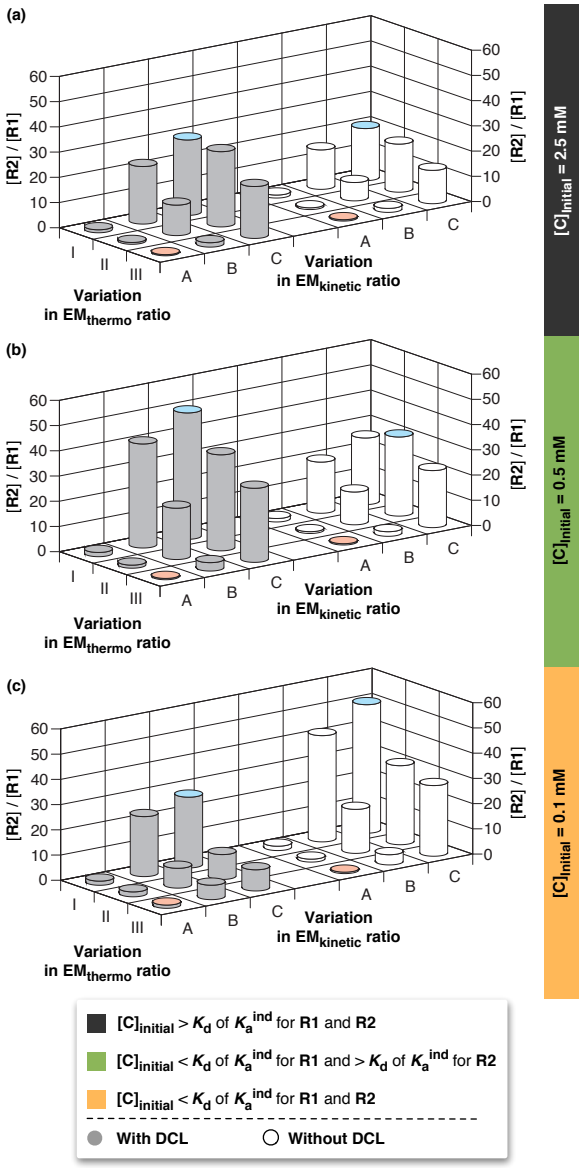

Figure 8. Outcome of kinetic simulations probing the influence of initial concentration (a, 2.5 mM; b, 0.5 mM; c, 0.1 mM), relative template duplex stability (EM_{thermo}, I to III), and relative template catalytic efficiency ($EM_{kinetic}$, A to C) on the ratio of [**R2**]/[**R1**] formed in the product pool in a dynamic system (gray cylinders) and in the absence of dynamically exchanging components (white cylinders), after two days. The conditions in which **R1** and **R2** exhibit the highest relative efficiency in terms of processing the reagent pool are highlighted in red and blue, respectively. Simulations were performed using the ISOSIM mode of the SimFit software package.

This difference manifests itself in a decrease in the [**R2**]/[**R1**] ratio at $[C]_{initial}$ of 0.1 mM in the DCL, since the concentration of **AZ** is now around 0.05 mM and, thus, lies well below the K_d of the individual binding events for both **R1** and **R2**. In the absence of the DCL, by contrast, this drastic dip in [**R2**]/[**R1**] ratio is not observed, as although the $[C]_{initial}$ is 0.1 mM and thus below the K_d of the individual binding events for both **R1** and **R2**, the processes involving **R2** (K_d = 0.33 mM) can operate more efficiently that those involving **R1** (K_d = 1.0 mM). In other

words, the critical threshold in terms of reagent concentration is not reached at this $[C]_{initial}$ in the absence of the DCL.

Moving away from the central simulation IIB, conditions IIA and IIC examine the effect of variation in the $EM_{kinetic}$. Specifically, they probe situations in which the values of k_{auto} for **R2** and **R1**, respectively, are decreased by a factor of 10 relative to their values in IIB. As a consequence, the ternary complex associated with one replicator or the other becomes more or less adept at catalyzing its own formation. Conditions IB and IIIB, on the other hand, simulate scenarios in which the values of K_a^{duplex} for **R2** and **R1**, respectively, are decreased by a factor of 10 relative to their values in IIB. The consequences of these changes are to make one replicator or the other more or less available in their catalytically-active monomeric forms. It is apparent from the results shown in Figure 8 that conditions IIA and IIIB are more favorable for the formation of **R1** than condition IIB, as evidenced by the decrease in the [**R2**]/[**R1**] ratio at all values of $[C]_{initial}$ examined. By contrast, in conditions IB and IIC, the formation of **R2** is more favored when compared to condition IIB, as evidenced by the increase in the [**R2**]/[**R1**] ratio under these conditions at all values of $[C]_{initial}$ examined. The highest selectivity for **R1**, however, is generally achieved under condition IIIA (Figure 8, highlighted in red), in which the ratio of $EM_{kinetic}$ for **R2**/**R1** is set to 10, and the relative duplex stability (ratio of EM_{thermo}) is 0.1. Clearly, therefore, out of all of the simulated conditions, replicator **R1** performs most efficiently in terms of its ability to process **AZ** for its own synthesis at the boundary condition where its catalytic efficiency is as high as possible and the stability of its template duplex is simultaneously as low as possible. Similarly, the highest selectivity for **R2** is achieved under condition IC (Figure 8, highlighted in blue), in which the ratio of $EM_{kinetic}$ for **R2**/**R1** is set to 0.1, and the relative duplex stability (ratio of EM_{thermo}) is 10. Therefore, **R2** also performs most efficiently at the boundary condition where its catalytic efficiency is as high as possible and the stability of its template duplex is simultaneously as low as possible.

In an ideal situation, irrespective of the presence or absence of a DCL, the output of the **R1**–**R2** replicator network would be associated with high overall conversions to recognition-mediated products **R1** and **R2**, resulting in a system dominated by replicators **R2** and **R1**, as opposed to unreacted starting materials or cycloadducts incapable of participating in recognition-mediated processes. In order to determine the influence of the three key parameters identified in Figure 7a on the outcome of processing the starting material pool in terms of conversion, we processed each simulated data set to determine the percentage overall conversion to all cycloadducts and proportion of **R1** and **R2** in the cycloadduct pool. The

results obtained for condition IIB across a range of $[C]_{initial}$ from 0.1 mM to 25 mM are shown in Figure 9 (for other conditions, see the Supporting Information).

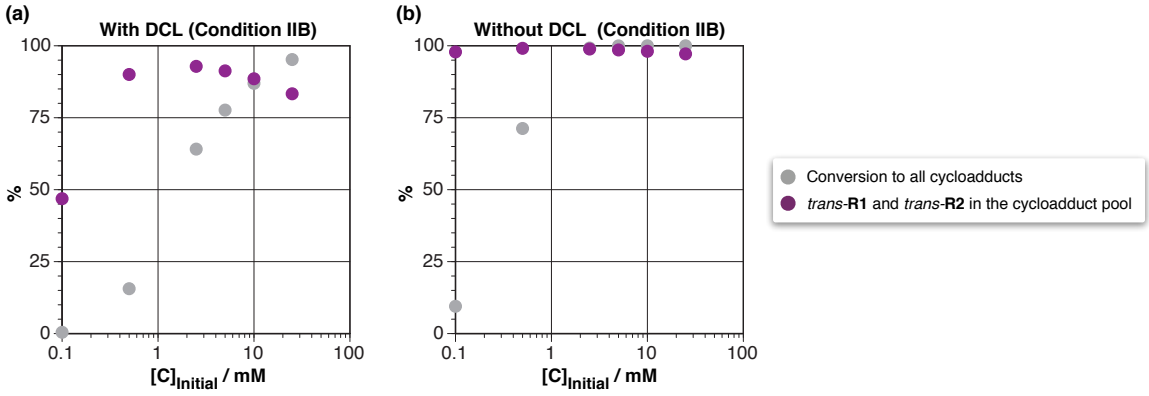

Figure 9. Outcome of kinetic simulations probing the influence of initial concentration in Condition IIB ($EM_{kinetic}$ and EM_{thermo} = 1) on the conversion to all cycloadducts (gray circles) and the % of the recognition-enabled **R1** and **R2** species in the cycloadduct product pool (purple circles) in (a) **R1**–**R2** network coupled to DCL after two days and (b) **R1**–**R2** in the absence of the DCL after two days. Simulations were performed using the ISOSIM mode of the SimFit software package. (a,b) Note that the *x*-axis is presented in logarithmic scale.

Analysis of these results reveals that under the majority of the $EM_{kinetic}$ and EM_{thermo} conditions examined here, the maximum proportion of the target replicators in the product pool is achieved within the $[C]_{initial}$ range of 2.5 to 10.0 mM. In condition IIB, the overall conversion to all cycloadducts falls below 25% within the DCL and below 75% in its absence when the $[C]_{initial}$ decreases below 1 mM. In addition, it is also apparent that the efficiencies of the recognition-mediated processes diminish as the $[C]_{initial}$ decreases or increases beyond the optimum window. The extent to which this affects the direction of the system toward **R1** and **R2** is considerably more significant in the network coupled to the DCL. At lower values of $[C]_{initial}$, this outcome can be attributed to the effective concentration of the key nitrone **AZ** being lower in the DCL than in its absence. By contrast, at $[C]_{initial}$ of 10 mM and above, the decrease in the proportion of recognition-mediated products in the product pool can be attributed to the higher contribution of unwanted bimolecular reaction pathways to the overall reaction flux. This trend is more substantial in the network simulated within the DCL, where in addition to the *cis*-**R1** and *cis*-**R2** recognition-disabled cycloadducts, the system can give rise to *trans* and *cis* recognition-disabled cycloadducts formed from nitrones **BZ**, **CZ**, and **DZ**. Taken together, therefore, the potential benefit afforded by utilizing $[C]_{initial}$ conditions of lower concentrations (*i.e.*, 0.1 and 0.5 mM) in terms of increased selectivity for a particular replicator over another, must be weighed carefully against the lower overall conversion to cycloadducts and the lower proportion of replicators **R1** and **R2** in the product pool that are obtained typically under such

conditions. That is, although the selectivity for one replicator over another might be enhanced, the reaction mixture is likely to be dominated by the starting materials or recognition-disabled products.

Conclusions

In conclusion, we have described a reaction network of two competing replicators that is coupled to a dynamic reagent pool that contains the components required for the syntheses of these replicators. In this coupled system, irreversible cycloadditions between two maleimides and the reactive nitrones present in the DCL, **AZ** to **DZ**, remove these compounds from the dynamic library permanently. The two replicators that are synthesized from **AZ** exploit recognition-mediated auto- and crosscatalytic pathways to drive their own formation by extracting **AZ** from the DCL at higher rates than the other nitrones. These replication processes drive re-equilibration of the DCL to replenish the **AZ** lost at the expense of the other nitrones, **BZ**, **CZ** and **DZ**. The addition of an instructional input in the form of preformed template(s) $\mathbf{T^p}$ and $\mathbf{T^m}$ directs the output of the reaction network—that is, the relative degree of processing accomplished by the two replicators. In the present experimental execution, the relative differences between the abilities of the replicators to process the reagent pool to their own advantage do not extend beyond, and are, in fact, somewhat smaller than those observed under conditions where network output is driven by kinetic selection only. Kinetic simulations demonstrate that several key rules govern the behavior of two competing replication processes under conditions where their formation is coupled tightly the processing of the DCL, and, thus, also the degree of processing of the reagent pool accomplished by the replicators. Specifically, the abilities of the replicators to process the reagent pool are influenced significantly by the interplay between three main parameters—the replicator kinetic parameters, thermodynamic parameters and the initial reagent concentrations. In the presence and in the absence of the DCL, networks of competing replicators are subject to a critical threshold in terms of reagent concentration. Operating below this threshold results in a decrease in the relative effectiveness of the replicators to process the reagent pool. Operating above this critical threshold produces amplification of the selectivity for one replicator over the other, but the level of this amplification depends on other parameters. As a result of the distribution of building blocks between the library members, this critical threshold is at a higher concentration in the presence of the DCL than in its absence. The selection of optimal conditions must also take into consideration the impact of the different recognition events associated with the replicators. As long as the initial reagent concentration is above the critical threshold, in order to achieve maximum selectivity for one replicator over another, it is necessary to

consider the K_d for the individual recognition elements associated with each replicator—the optimum operational concentration for a network is likely to be at or close to the lower of these two K_d values. This observation can be used as an important design element for optimizing the performance of other replicator networks that are coupled to DCLs. In particular, the present experimental implementation can be viewed as non-optimized when it comes to achieving maximum selectivity for one replicator over another, as the two replicators generally co-exist. Consequently, we use kinetic simulations to map out additional outputs that are accessible to this system, yet might be challenging to attain experimentally through structural modification. These outputs can help us understand how the changes in the network genotype, *i.e.*, the strengths of the various catalytic pathways, affect the network phenotype—that is, the distribution of the replicator populations that are formed in the system. Ultimately, the combination of experimental and theoretical work described here allows us to identify the requirements necessary for the processing of a dynamic pool of chemical feedstock by a network of interconnected replicators in a programmed, but self-directed, manner to afford a desired network outcome (for example, a significant preference for one replicator over the other). The comparison of the network behavior observed in the presence and in the absence of the DCL highlights that the ability of one replicator to dominate within this network does not depend solely on the network genotype but also on the reaction environment in which it operates. As a result, the design framework presented here, together with the elucidation of the rules that govern its behavior, can be applied to the development of reaction networks with enhanced capacities to process reagent pools in programmed ways, as well as a platform to facilitate the study of replicator networks coupled to dynamic processes under flow conditions where continuous input and output of reagents—a change in the reaction environment—contribute to and broaden the spectrum of outputs accessible to a given network's genotype. These studies are currently in progress in our laboratory.

ASSOCIATED CONTENT

Supporting Information

Details of sample preparation, NMR analyses, kinetic simulations and scripts.

Author Information

Present Address (T. K. and D. P.): Department of Chemistry, Northwestern University, 2145 Sheridan Road, Evanston, IL 60208-3113, USA.

Corresponding author email: douglas.philp@northwestern.edu.

ORCID iDs:

DP: orcid.org/0000-0002-9198-4302

TK: orcid.org/0000-0001-7886-9660

Acknowledgements

This work was supported by the award of a Postgraduate Studentship from Engineering and Physical Sciences Research Council (EP/K503162/1) to TK and by the University of St Andrews.

Notes and references

(1) (a) Islam, S.; Powner, M. W. Prebiotic systems chemistry: complexity overcoming clutter. *Chem* **2017**, *2*, 1–32. (b) Ruiz-Mirazo, K.; Briones, C.; de la Escosura, A. Prebiotic systems chemistry: new perspectives for the origins of life. *Chem. Rev.* **2014**, *114*, 285–366. (c) Blackmond, D. G. The origin of biological homochirality. *Cold. Spring Harb. Perspect. Biol.* **2010**, *2*:a002147. (d) Pross, A. Seeking the chemical roots of Darwinism: bridging between chemistry and biology. *Chem. Eur. J.* **2009**, *15*, 8374–8391. (e) Rauchfuss, H. In: *Chemical Evolution and the Origin of Life*; Mitchell, T. N. Ed.; Springer: Berlin, 2008. (f) Newman, M. E. J. The structure and function of complex networks. *SIAM Rev.* **2003**, *45*, 167–256.

(2) (a) Sutherland, J. D. Opinion: studies on the origin of life—the end of the beginning. *Nat. Rev. Chem.* **2017**, *1*, 0012. (b) Pross, A.; Pascal, R. How and why kinetics, thermodynamics, and chemistry induce the logic of biological evolution. *Beilstein. J. Org. Chem.* **2017**, *13*, 665–674. (c) Ruiz-Mirazo, K.; Moreno, A. Reflections on the origins of life. *Metode Sci. Stud. J.* **2016**, *6*, 151–159. (d) Sutherland, J. D. The origin of life—out of the blue. *Angew. Chem., Int. Ed.* **2015**, *55*, 104–121. (e) Mann, S. The origins of life: old problems, new chemistries. *Angew. Chem., Int. Ed.* **2013**, *52*, 155–162. (f) Deamer, D.; Weber, A. L. Bioenergetics and life's origins. *Cold Spring Harb. Perspect. Biol.* **2010**, *2*:a004929. (g) Peretó, J. Controversies on the origin of life. *Int. Microbiol.* **2005**, *8*, 23–31.

(3) (a) Higgs, P. G.; Lehman, N. The RNA world: molecular cooperation at the origins of life. *Nat. Rev. Genet.* **2015**, *16*, 7–17. (b) Neveu, M.; Kim, H.-J.; Benner, S. A. The "strong" RNA world hypothesis: fifty years old. *Astrobiology* **2013**, *13*, 391–403. (c) Vaidya, N.; Manapat, M. L.; Chen, I. A.; Xulvi-Brunet, R.; Hayden, E. J.; Lehman, N. Spontaneous network formation among cooperative RNA replicators. *Nature* **2012**, *491*, 72–77. (d) Danger, G.; Plasson, R.; Pascal, R. Pathways for the formation and evolution of peptides in prebiotic environments. *Chem. Soc. Rev.* **2012**, *41*, 5416–5429. (e) Szostak, J. W. The eightfold path to non-enzymatic RNA replication. *J. Syst. Chem.* **2012**, *3*, 2. (f) Robertson, M. P.; Joyce, J. F. The origins of the RNA world. *Cold Spring Harb. Perspect. Biol.* **2012**, *4*:a003608. (g) Fry, I. The role of natural selection in the origin of life. *Origins Life Evol. Biospheres* **2011**, *41*, 3–16. (h) Kauffman, S. A. Approaches to the origin of life on Earth. *Life* **2011**, *1*, 34–38. (i) Joshi, P. C.; Aldersley, M. F.; Delano, J. W.; Ferris, J. P. Mechanism of montmorillonite catalysis in the

formation of RNA oligomers. *J. Am. Chem. Soc.* **2009**, *131*, 13369–13374. (j) Eschenmoser, A. The search for the chemistry of life's origin. *Tetrahedron* **2007**, *63*, 12821–12844. (k) Luisi, P. L. *The Emergence of Life*; Cambridge University Press, 2006. l) Segré, D.; Ben-Eli, D.; Deamer, D. W.; Lancet, D. The lipid world. *Orig. Life Evol. Biosph.* **2001**, *31*, 119–145.

(4) (a) Muchowska, K. B.; Varma, S. J.; Chevallot-Beroux, E.; Lethuillier-Karl, L.; Li, G.; Moran, J. Metals promote sequences of the reverse Krebs cycle. *Nat. Ecol. Evol.* **2017**, *1*, 1716–1721. (b) Peretó, J. Out of fuzzy chemistry: from prebiotic chemistry to metabolic networks. *Chem. Soc. Rev.* **2012**, *41*, 5394–5403. (c) Shapiro, R. Small molecule interactions were central to the origin of life. *Q. Rev. Biol.* **2006**, *81*, 105–125. (d) Smith, E.; Morowitz, H. J. Universality in intermediary metabolism. *Proc. Natl. Acad. Sci. U. S. A.* **2004**, *101*, 13168–13173. (e) Orgel, L. E. Self-organizing biochemical cycles. *Proc. Natl. Acad. Sci. U. S. A.* **2000**, *97*, 12503–12507.

(5) (a) Ruiz-Mirazo, K.; Briones, C.; de la Escosura, A. Chemical roots of biological evolution: the origins of life as a process of development of autonomous functional systems. *Open Biol.* **2017**, *7*, 170050. (b) Powner, M. W.; Sutherland, J. D. Prebiotic chemistry: a new modus operandi. *Phil. Trans. R. Soc. B* **2011**, *366*, 2870–2877. (c) Lazcano, A. Historical development of origins research. *Cold Spring Harbor Perspect. Biol.* **2010**, *2*:a002089. (d) Szathmáry, E. The origin of replicators and reproducers. *Phil. Trans. R. Soc. B* **2006**, *361*, 1761–1776. (e) Dyson, F. *Origins of Life*; Cambridge University Press: Cambridge, 2004. (f) Mason, S. F. *Chemical Evolution*; Oxford University Press Inc.: New York, 1991. (g) Cairns-Smith, A. G. *Seven Clues to the Origin of Life*; Cambridge University Press: Cambridge, 1985. (h) Orgel, L. E. *The Origins of Life*; John Wiley & Sons, Inc.: USA, 1973.

(6) (a) Kosikova, T.; Philp, D. Exploring the emergence of complexity using synthetic replicators. *Chem. Soc. Rev.* **2017**, *46*, 7274–7305. (b) Duim, H.; Otto, S. Towards open-ended evolution in self-replicating molecular systems. *Beilstein. J. Org. Chem.* **2017**, *13*, 1189–1203. (c) Bissette, A. J.; Fletcher, S. P. Mechanism of autocatalysis. *Angew. Chem., Int. Ed*. **2013**, *52*, 12800–12826. (d) Philp, D.; Huck, J. Supramolecular Chemistry: From Molecules to Nanomaterials; John Wiley & Sons, Ltd.: New York, 2012; Vol. 4, pp. 1415–1445. (e) Vidonne, A.; Philp, D. Making molecules that make themselves—the chemistry of artificial replicators. *Eur. J. Org. Chem*. **2009**, *2009*, 593–583. (f) Patzke, V.; von Kiedrowski, G. Self replicating systems. *ARKIVOC* **2007**, *46*,

293–310. (g) von Kiedrowski, G. Minimal Replicator Theory I: Parabolic Versus Exponential Growth. In: *Bioorganic Chemistry Frontiers*; Dugas, H.; Schmidtchen, F. P., Eds.; Springer: Berlin, Heidelberg, 1993, Vol. 3, pp. 113–146.

(7) For examples of self-replicators in isolation, see: (a) Plöger, T. A.; von Kiedrowski, G. A self-replicating peptide nucleic acid. *Org. Biomol. Chem.* **2014**, *12*, 6908–6914. (b) Dieckmann, A.; Beniken, S.; Lorenz, S.; Doltsinis, N. L.; von Kiedrowski, G. Unravelling a fulvene based replicator: experiment and theory in interplay. *J. Syst. Chem.* **2010**, *1*, 10. (c) Carnall, J. M. A.; Waudby, C. A.; Belenguer, A. M.; Stuart, M. C. A.; Peyralans, J. J.-P.; Otto, S. Mechanosensitive self-replication driven by self-organization. *Science* **2010**, *327*, 1502–1506. (d) Kassianidis, E.; Philp, D. Design and implementation of a highly selective minimal self-replicating system. *Angew. Chem., Int. Ed.* **2006**, *45*, 6344–6348. (e) Issac, R.; Chmielewski, J. Approaching exponential growth with a self-replicating peptide. *J. Am. Chem. Soc.* **2002**, *124*, 6808–6809. (f) Paul, N.; Joyce, G. F. A self-replicating ligase ribozyme. *Proc. Natl. Acad. Sci. U. S. A.* **2002**, *99*, 12733–12740. (g) Wang, B.; Sutherland, I. O. Self-replication in a Diels–Alder reaction. *Chem. Commun.* **1997**, *0*, 1495–1496. (h) Lee, D. H.; Granja, J. R.; Martinez, J. A.; Severin, K.; Ghadri, M. R. A self-replicating peptide. *Nature* **1996**, *382*, 525–528. (i) Tjivikua, T.; Ballester, P.; Rebek, J., Jr. Self-replicating system. *J. Am. Chem. Soc.* **1990**, *112*, 1249–1250. (j) Zielinski, W. S.; Orgel, L. E. Autocatalytic synthesis of a tetranucleotide analogue. *Nature* **1987**, *327*, 346–347. (k) von Kiedrowski, G. A self-replicating hexadeoxynucleotide. *Angew. Chem., Int. Ed. Engl.* **1986**, *25*, 932–935.

(8) For examples of reciprocal replicators in isolation, see: (a) Robertson, C. C.; Mackenzie, H. W.; Kosikova, T.; Philp, D. An environmentally responsive reciprocal replicating network. *J. Am. Chem. Soc.* **2018**, *140*, 6832–6841. (b) Lincoln, T. A.; Joyce, G. F. Self-sustained replication of an RNA enzyme. *Science* **2009**, *323*, 1229–1232. (c) Kassianidis, E.; Philp, D. Reciprocal template effects in a simple synthetic system. *Chem. Commun.* **2006**, 4072–4074. (d) Kim, D.-E.; Joyce, G. F. Cross-catalytic replication of an RNA ribozyme. *Chem. Biol.* **2004**, *11*, 1505–1512. (e) Pieters, R. J.; Huc, I.; Rebek, J., Jr Reciprocal template effects in bisubstrate systems: A replication cycle. *Tetrahedron* **1995**, *51*, 485–498. (f) Pieters, R. J.; Huc, I.; Rebek, J., Jr. Reciprocal template effects in a replication cycle. *Angew. Chem., Int. Ed. Engl.* **1994**, *33*, 1579–1581. (g) Inoue, T.; Joyce, G. F.; Grzeskowiak, K.; Orgel, L. E.; Brown, J. M.; Reese, C. B. Template-directed synthesis on the pentanucleotide CpCpGpCpC. *J. Mol. Biol.* **1984**,

178, 669–676. (h) Orgel, L. E.; Lohrmann, R. Prebiotic chemistry and nucleic acid replication. *Acc. Chem. Res.* **1974**, *7*, 368–377.

(9) (a) Sadownik, J. W.; Kosikova, T.; Philp, D. Generating system-level responses from a network of simple synthetic replicators. *J. Am. Chem. Soc.* **2017**, *139*, 17565–17573. (b) Kassianidis, E.; Pearson, R. J.; Wood, E. A.; Philp, D. Designing instructable networks using synthetic replicators. *Faraday Discuss*. **2010**, *145*, 235–254. (c) Dadon, Z.; Wagner, N.; Ashkenasy, G. The road to non-enzymatic molecular networks. *Angew. Chem., Int. Ed.* **2008**, *47*, 6128–6138. (d) Ashkenasy, G.; Jagasia, R.; Yadav, M.; Ghadiri, M. R. Design of a directed molecular network. *Proc. Natl. Acad. Sci. U. S. A.* **2004**, *101*, 10872–10877. (e) Yao, S.; Ghosh, I.; Zutshi, R.; Chmielewski, J. Selective amplification by auto- and cross-catalysis in a replicating peptide system. *Nature* **1998**, *396*, 447–450. (f) Sievers, D.; von Kiedrowski, G. Self-replication of hexadeoxynucleotide analogues: autocatalysis versus cross-catalyssis. *Chem. – Eur. J.* **1998**, *4*, 629–641

(10) (a) Samiappan, M.; Dadon, Z.; Ashkenasy, G. Replication NAND gate with light as input and output. **2011**, *47*, 710–712. (b) Ashkenasy, G.; Dadon, Z.; Alesebi, S.; Wagner, N.; Ashkenasy, N. Building logic into peptide networks: bottom-up and top-down. *Isr. J. Chem.* **2011**, *51*, 106–117. (c) Allen, V. C.; Robertson, C. C.; Turega, S. M.; Philp, D. A simple network of synthetic replicators can perform the logical OR operation. *Org. Lett.* **2010**, *12*, 1920–1923. (d) Dadon, Z.; Samiappan, M.; Safranchik, E. Y.; Ashkenasy, G. Light-induced peptide replication controls logic operations in small networks. *Chem. – Eur. J.* **2010**, *16*, 12096–12099 (e) Ashkenasy, G.; Ghadiri, M. R. Boolean logic functions of a synthetic peptide network. *J. Am. Chem. Soc.* **2004**, *126*, 11140–11141.

(11) Severin, K.; Lee, D. H.; Martinez, J. A.; Vieth, M.; Ghadiri, M. R. Dynamic error correction in autocatalytic peptide networks. *Angew. Chem., Int. Ed. Engl.* **1998**, *37*, 126–128.

(12) (a) Kindermann, M.; Stahl, I.; Reimold, M.; Pankau, W. M.; von Kiedrowski, G. Systems chemistry: kinetic and computational analysis of a nearly exponential organic replicator. *Angew. Chem., Int. Ed.* **2005**, *44*, 6750–6755. (b) Saghatelian, A.; Yokobayashi, Y.; Soltani, K.; Ghadiri, M. R. A chiroselective peptide replicator. *Nature* **2001**, *409*, 797–801.

(13) (a) Vidonne, A.; Kosikova, T.; Philp, D. Exploiting recognition-mediated assembly and reactivity in [2]rotaxane formation. *Chem. Sci.* **2016**, *7*, 2592–2603. (b) Kosikova, T.; Hassan, N. I.; Cordes, D. B.; Slawin, A. M. Z.; Philp, D. Orthogonal recognition

processes drive the assembly and replication of a [2]rotaxane. *J. Am. Chem. Soc.* **2015**, *137*, 16074–16083. (c) Vidonne, A.; Philp, D. Integrating replication processes with mechanically interlocked molecular architectures. *Tetrahedron* **2008**, *64*, 8464–8475.

(14) (a) Bottero, I.; Huck, J.; Kosikova, T.; Philp, D. A synthetic replicator drives a propagating reaction–diffusion front. *J. Am. Chem. Soc.* **2016**, *138*, 6723–6726. For an example of a reaction-diffusion front driven by autocatalysis in an enzymatic reaction network, see: (b) Semenov, S. N.; Markvoort, A. J.; de Greef, T. F. A.; Huck, W. T. S. Threshold sensing through a synthetic enzymatic reaction-diffusion network. *Angew. Chem., Int. Ed.* **2014**, *53*, 8066–8069. For an example of spatial waves in a biochemical network, see: (c) Padirac, A.; Fujii, T.; Estévez-Torres, A.; Rondelez, Y. Spatial waves in synthetic biochemical networks. *J. Am. Chem. Soc.* **2013**, *135*, 14586–14592.

(15) (a) *Dynamic Covalent Chemistry: Principles, Reactions, and Applications*; Zhang, W., Jin, Y., Eds.; John Wiley & Sons, Inc.: Hoboken, NJ, 2018. (b) Hermann, A. Dynamic combinatorial/covalent chemistry: a tool to read, generate and modulate the bioactivity of compounds and compound mixtures. *Chem. Soc. Rev.* **2014**, *43*, 1899–1933 (c) Jin, Y.; Yu, C.; Denman, R. J.; Zhang, W. Recent advances in dynamic covalent chemistry. *Chem. Soc. Rev.* **2013**, *42*, 6634–6654. (d) Belowich, M. E.; Stoddart, J. F. Dynamic imine chemistry. *Chem. Soc. Rev.* **2012**, *41*, 2003–2024. (e) Constitutional Dynamic Chemistry. In: *Topics in Current Chemistry*; Barboiu, M., Ed.; Springer-Verlag: Berlin, Heidelberg, 2012, Vol. 322, pp. 1–320. (f) Sadownik, J. W.; Uljin, R. V. Dynamic covalent chemistry in aid of peptide self-assembly. *Curr. Opin. Biotechnol.* **2010**, *21*, 401–411. (g) Gasparini, G.; Dal Molin, M.; Prins, L. J. Dynamic approaches towards catalyst discovery. *Eur. J. Org. Chem.* **2010**, 2429–2440. (h) Corbett, P. T.; Leclaire, J.; Vial, L.; West, K. R.; Wietor, J.-L.; Sanders, J. K. M.; Otto, S. Dynamic combinatorial chemistry. *Chem. Rev.* **2006**, *106*, 3652–3711. (i) Rowan, S. J.; Cantrill, S. J.; Cousins, G. R. L.; Sanders, J. K. M.; Stoddart, J. F. Dynamic covalent chemistry. *Angew. Chem., Int. Ed.* **2002**, *41*, 898–952.

(16) (a) Li, J.; Nowak, P.; Otto, S. Dynamic combinatorial libraries: from exploring molecular recognition to systems chemistry. *J. Am. Chem. Soc.* **2013**, *135*, 9222–9239. (b) Hunt, R. A. R.; Otto, S. Dynamic combinatorial libraries: new opportunities in systems chemistry. *Chem. Commun.* **2011**, *47*, 847–858. (c) Miller, B. L. Catalysing dynamic libraries. *Nat. Chem.* **2010**, *2*, 433–434. (d) del Amo, V.; Philp, D. Integrating replication-based selection strategies in dynamic covalent systems. *Chem. – Eur. J.*

2010, *16*, 13304–13318. (e) Turega, S. M.; Lorenz, C.; Sadownik, J. W.; Philp, D. Target-driven selection in a dynamic nitrone library. *Chem. Commun.* **2008**, *0*, 4076–4078. (f) Brisig, B. B.; Sanders, J. K. M.; Otto, S. Selection and amplification of a catalyst from a dynamic combinatorial library. *Angew. Chem., Int. Ed.* **2003**, *42*, 1270–1273.

(17) For studies where replication processes within DCL operate reversibly, see: (a) Dadon, Z.; Wagner, N.; Alasibi, S.; Samiappan, M.; Mukherjee, R.; Ashkenasy, G. Competition and cooperation in dynamic replication networks. *Chem. – Eur. J.* **2015**, *21*, 648–654. (b) Dadon, Z.; Samiappan, M.; Wagner, N.; Ashkenasy, G. Chemical and light triggering of peptide networks under partial thermodynamic control. *Chem. Commun*. **2012**, *48*, 1419–1421. (c) del Amo, V.; Slawin, A. M. Z.; Philp, D. Modulating replication processes within a dynamic covalent framework. *Org. Lett.* **2008**, *10*, 4589–4592. (d) Xu, S.; Giuseppone, N. Self-duplicating amplification in a dynamic combinatorial library. *J. Am. Chem. Soc.* **2008**, *130*, 1826–1827. (e) Terfort, A.; von Kiedrowski, G. Self-replication by condensation of 3-aminobenzamidines and 2-formylphenoxyacetic acids. *Angew. Chem., Int. Ed.* **1992**, *31*, 654–656. For other examples where self-assembly processes that are essential for replication may affect exchange rates, see (f) Bartolec, B.; Altay, M.; Otto, S. Template-promoted self-replication in dynamic combinatorial libraries made from a simple building block. *Chem. Commun.* **2018**, *54*, 13096–13098. (g) Sadownik, J. W.; Mattia, E.; Nowak, P.; Otto, S. Diversification of self-replicating molecules. *Nat. Chem.* **2016**, *8*, 264–269. (h) Leonetti, G.; Otto, S. Solvent composition dictates the emergence in dynamic molecular networks containing competing replicators. *J. Am. Chem. Soc.* **2015**, *137*, 2067–2072.

(18) For a study where replication processes within DCL operate irreversibly, see: Sadownik, J. W.; Philp, D. A simple synthetic replicator amplifies itself from a dynamic reagent pool. *Angew. Chem., Int. Ed.* **2008**, *47*, 9965–9970.

(19) (a) Kosikova, T.; Mackenzie, H.; Philp, D. Probing the limits of selectivity in a recognition-mediated reaction network embedded within a dynamic covalent library. *Chem. – Eur. J.* **2016**, *22*, 1831–1839. (b) Sadownik, J. W.; Philp, D. A recognition-mediated reaction drives the amplification within a dynamic library. *Org. Biomol. Chem.* **2015**, *13*, 10392–10401.

(20) The superscript p in $\mathbf{M^p}$ and $\mathbf{T^p}$ denotes the location of the carboxylic acid recognition site on a methylene carbon *para* to the maleimide and isoxazolidine cycloadduct rings, respectively. By contrast, superscript m in $\mathbf{M^m}$ and $\mathbf{T^m}$ denotes the presence of a

carboxylic acid attached directly to the benzene ring in position *meta* relative to the maleimide and isoxazolidine cycloadduct rings, respectively. The syntheses and characterizations of maleimide **M**$^{\mathbf{m}}$ and replicators **T**$^{\mathbf{p}}$ and **T**$^{\mathbf{m}}$ are reported in Ref. [21].

(21) Kosikova, T.; Philp, D. A critical cross-catalytic relationship determines the outcome of competition in a replicator network. *J. Am. Chem. Soc.* **2017**, *139*, 12579–12590; this works reports the comprehensive kinetic analyses of the various recognition-disabled, autocatalytic, and cross-catalytic pathways pertaining to replicators *trans*-**T**$^{\mathbf{p}}$ and *trans*-**T**$^{\mathbf{m}}$.

(22) For details of $^{19}F\{^{1}H\}$ NMR spectroscopy experiments, their subsequent deconvolution, and determination of associated errors, see the Supporting Information.

(23) The 1,3-dipolar cycloaddition reaction between a maleimide and a nitrone can produce two diastereoisomers labeled *trans* and *cis*. These two labels refer to the relative configuration of the three protons located on the isoxazolidine ring of the cycloadduct. In the absence of recognition-mediated processes, the ratio of *trans* to *cis* is typically 3:1 (See, for example, references 7d and 21).

(24) In the reaction network incorporating **T**$^{\mathbf{p}}$ and **T**$^{\mathbf{m}}$ replicators, only the *trans* diastereoisomers formed by the reactions of **AZ** with **M**$^{\mathbf{p}}$ and **AZ** with **M**$^{\mathbf{m}}$ are capable of taking part in template-directed replication processes. Consequently, the notation for the *trans* cycloadducts capable of replication generally omits the "*trans*" (**T**$^{\mathbf{p}}$ is synonymous with *trans*-**T**$^{\mathbf{p}}$ and **T**$^{\mathbf{m}}$ is synonymous with *trans*-**T**$^{\mathbf{m}}$).

(25) (a) Sadownik, J. W. Evolving Complex Systems from Simple Molecules. PhD Dissertation, University of St Andrews, St Andrews, 2009. (b) Turega, S. M.; Lorenz, C.; Sadownik, J. W.; Philp, D. *Chem. Commun.* **2008**, 4076–4078.

(26) Only the concentrations of **Z** and the azoxy side product, *i.e.*, the two species that were present after two days at very low concentrations of <0.1 mM changed by more than 5% when the DCL compositions were compared after two and seven days. The azoxy side-product shown in Figure 2 (marked with a star) is formed by oxidation of hydroxylamine **Z** to the corresponding nitroso compound, and its subsequent reaction with hydroxylamine **Z** itself.

(27) The preformed templates used in the template-instructed DCL experiments consist solely of the *trans* diastereoisomer of the relevant replicator.

(28) The ratios obtained under kinetic selection only (*i.e.*, in the absence of a DCL) after 16 h were: 1.13 (no T), 0.80 (**T**$^{\mathbf{p}}$), 1.58 (**T**$^{\mathbf{m}}$), and 0.93 (both **T**$^{\mathbf{p}}$ and **T**$^{\mathbf{m}}$) (Data taken from Ref. [21]).

(29) The exchange reactions employed in this work occur at much faster rates than the cycloaddition reactions (*i.e.*, the cycloaddition reactions are rate-limiting). When replicators operate in a dynamic covalent library where the exchange rates are slower than the irreversible reactions forming the replicators, the population of replicators reflects library composition rather than expressing the kinetic genotype of the replicator network. See, Mackenzie, H. *Overcoming Limited Selectivity in Recognition-Mediated Replicating Systems*. M. Phil. Thesis, University of St Andrews, St Andrews, 2011.

(30) For results of simulations performed at $[C]_{initial}$ = 5–25 mM, please see Figure S5.

For ToC Graphic only:

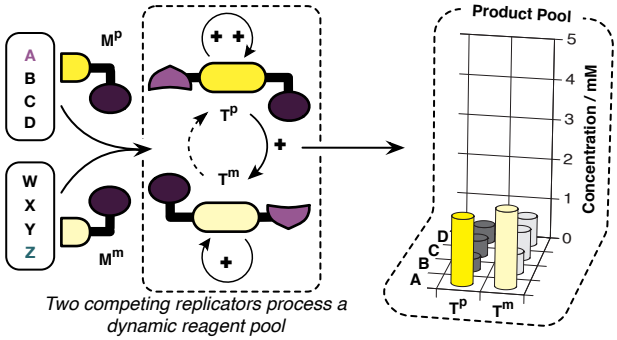

Two competing replicators process a dynamic reagent pool